JOURNAL OF MATERIALS SCIENCE 32 (1997) 4493–4500

Mechanical property characterization of a number of polymers using uniaxial compression and spherical tipped indentation tests

G. KOURTESIS, G. M. RENWICK, A. C. FISCHER-CRIPPS*
*Departments of Materials Science and *Physics, University of Technology, Sydney Broadway, NSW 2007, Australia*

M. V. SWAIN
CSIRO Division of Applied Physics, Lindfield NSW 2070 and Department of Mechanical Engineering, University of Sydney, NSW 2006, Australia

A number of thermoplastic polymers have been tested in uniaxial compression and by monitoring the force–displacement response of small spherical indenters loaded into the surface. The compression tests were performed using a conventional universal testing machine while the very small diamond indenters, of nominal 20 and 50 μm radius, were impressed only a few micrometres into the surface with a high precision micromechanical probe. Results from the two approaches are compared and discussed in terms of the proposed relationships between hardness or contact pressure and yield stress for the considered polymers.

1. Introduction

Indentation has long been used as a simple means for estimating the mechanical properties of metals. Hardness or contact pressure, about which international standards have been established, is often used as a means of defining the plastic penetration resistance or yield stress of a metallic material. In recent years there have been significant advances in the measuring instruments so that with modern micromechanical probe systems, contact pressure or hardness as well as elastic modulus measurements may be made at submicrometer or even nanometer dimensions [1, 2].

Although hardness standards exist for rubbers and polymers, they are not a widely reported property. This arises because of the difficulty of accurately measuring the residual impression, although some test procedures such as the Durometer (Shore A, etc.) and Barcol [3] do monitor the change in depth of penetration of an indenter for an increment of force, from which a measure of "hardness" is obtained. In the case of elastomeric materials, the latter value is more indicative of the modulus than the plastic response. A critical review of this topic has recently been presented by Briscoe and Sebastian [4].

Ion *et al.* [5] recently published a study of the behaviour of an amorphous and drawn polyethylene terephthalate (PET) upon indentation with a micromechanical probe using a corner cube pointed indenter, with an apical angle of 35°. Despite such a sharp indenter these authors found only a minor contribution to the penetration depth caused by creep. The strong temperature sensitivity of the visco-elastic behaviour, particularly at temperatures approaching the glass transition temperature, T_g, often leads to difficulties in interpreting force–displacement curves generated using micromechanical probes particularly for the determination of hardness and modulus. Ni *et al.* [6] have applied finite element methods to assist with the interpretation of such force–displacement curves for gelatin based films widely used for photographic purposes.

The use of hardness or contact pressure to determine the yield stress of materials has had a long history for metals and some involvement but less independent verification for polymers, ceramics and inorganic glasses. Tabor [7], summarizing a wealth of existing data, showed that for ductile metals the hardness, H, and yield stress, σ_y, could be related by the simple relationship

$$H = C\sigma_y \quad (1)$$

where $C \sim 2.8$, is a constant. Subsequent research by Marsh [8] attempted to extend this type of relationship to less ductile materials such as glasses, for which no other simple measure of yield stress was available. Marsh utilized a spherical cavity elastic–plastic solution developed by Hill [9] to relate the hardness and yield stress for such materials. Later Hirst and Howse [10] extended the concept to that of indentation of polymers with wedges of different included angles. Both Marsh and Hirst and Howse suggested that for materials with high hardness to modulus (H/E) ratios

0022–2461

the constant C in Equation 1 was less than 2.8. A unifying approach for the determination of the constant C for metals, polymers and glasses was suggested by Johnson [11], by further extension of the spherical cavity model. He proposed the following relationship between hardness, modulus, yield stress, indenter geometry and the constant C, namely

$$H/\sigma_y = C = 2/3[2 + \ln(0.33E/\sigma_y \tan\beta)] \quad (2)$$

where E is the elastic modulus and β is the indenter complimentary angle (between indenter face and specimen surface). This relationship is plotted in Fig. 1a, and shows that for one material (E/σ_y = constant) the value of C(H/σ_y) may change from one to three, depending upon the indenter angle. As Johnson showed, a better fit to a wide range of existing data for materials with different σ_y/E ratios could be obtained by a more general relationship, namely

$$H/\sigma_y = C = A + B\ln(0.33E/\sigma_y \tan\beta) \quad (3)$$

with A and B constants ($\sim 5/4$ and 2/3, respectively). The above relationships both explicitly include σ_y; however, for a Vickers (or Berkovich) indenter with $\beta = 19.7^\circ$, the above expression may be manipulated so that a plot of H/σ_y (or C) versus E/H may be obtained as shown in Fig. 1b. This figure indicates that over a wide range of E/H, including most polymers, C is dependent upon E/H. For spherical tipped indenters Johnson [11], following Tabor [7], proposed that

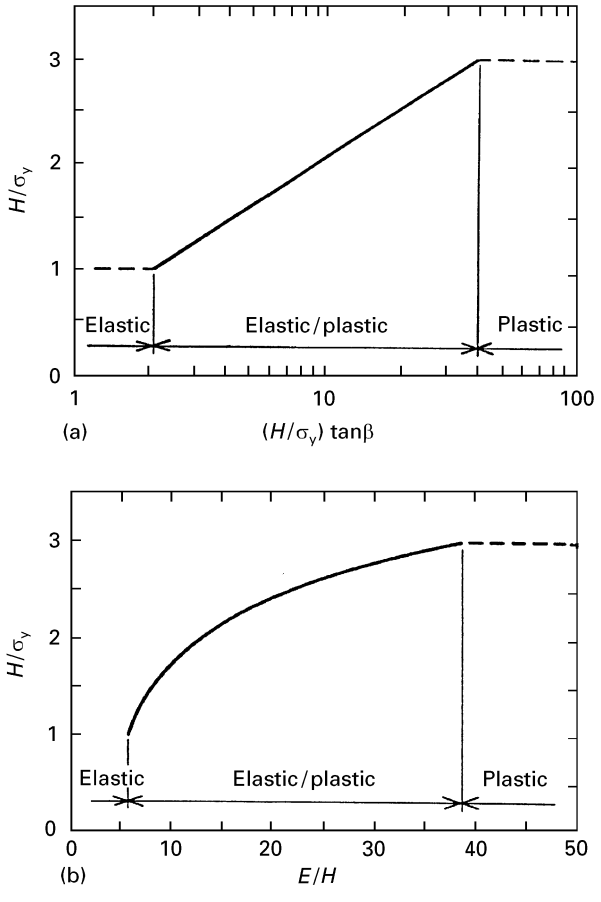

Figure 1 (a) Plot of the ratio H/σ_y versus $(E/\sigma_y)\tan\beta$ from Equation 2. (b) The same plot, but for a Vickers or Berkovich indenter ($\beta = 19.7^\circ$).

$\tan\beta = a/R$, where a is the contact radius and R the indenter radius.

An alternative approach that models the deformation beneath an indenter was proposed by Shaw and DeSalvo [12] about the same time as Johnson. This model considers a much more constrained plastic deformation beneath the indenter; in fact the plastic zone does not escape from beneath the area of contact. Yoffe [13], using a simple analysis of pointed indentation, indicated that the stress distribution in the vicinity of the contact area was very different to that of the proposed spherical cavity model of Johnson [11]. Fischer–Cripps [14] has recently compared experimental observations of the deformed zone beneath spherical indentations in glass ceramics and finite element mechanics (FEM) models based on the Tresca yield criteria. The predicted zones are close to those proposed by Shaw and DeSalvo [12] for high values (> 0.1) of H/E and close to the experimental observations of the deformation zone beneath a spherical indenter for glass ceramics. These FEM predictions of the constrained plastic zone are also very similar to the zones observed in polymeric materials by Puttick *et al.* [15].

The approaches developed above, particularly the spherical cavity model, have been applied to polymers and glasses despite the analysis being based on an elastic perfectly plastic constitutive relationship more applicable for metals. The appropriate relationship for flow in polymers and glasses is generally much more complex with the former exhibiting a visco-elastic component and both showing pressure sensitivity, that is, the yield stress dependence upon the confining pressure. A more critical appraisal of the elastic–plastic response to generalized loading of polymeric materials has been developed by Argon [16]. This development was utilized by Kent [17] who investigated the indentation response of polymethyl metacrylate (PMMA) and incorporated the influence of visco-elastic and pressure sensitivity in a simple manner using the following expression

$$\sigma_y = \sigma_y^0 + X\ln\dot{\varepsilon} + YP \quad (4)$$

where σ_y^0 is the constraint free yield stress, X and Y are constants, $\dot{\varepsilon}$ is the radial strain rate and P is the hydrostatic pressure. The hydrostatic pressure, P, is given by

$$P = (\sigma_{xx} + \sigma_{yy} + \sigma_{zz})/3 \quad (5)$$

and σ_{ii} are the three principal stresses. For a uniaxial tensile test $P = -\sigma_t/3$, for a uniaxial compression test, $P = \sigma_c/3$, and beneath a spherical indenter $P \sim p_0(x/a, z/a)$ where p_0 is the average contact pressure and x the radial distance and z the vertical distance both normalized to the contact radius, a. A more critical consideration of the elastic shear stress distribution beneath a spherical tipped indenter with and without the hardening influence of the hydrostatic pressure on the contours of deviatoric shear stress is shown in Fig. 2. The upper plot (Fig. 2a) shows the Tresca shear stress distribution with X and Y in Equation 4 set to zero for a sphere in contact with a flat. The maximum shear stress is $\sim 0.87p_0$ and it occurs on

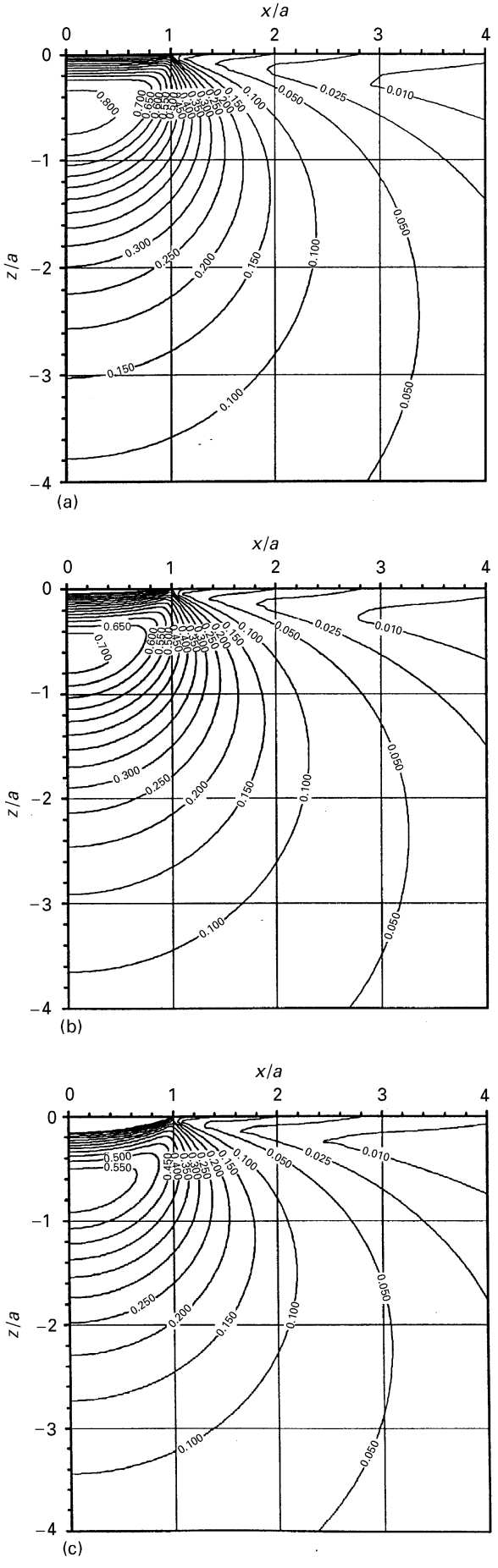

Figure 2 Plots of the Tresca shear stress distributions beneath a spherical indenter with and without the influence of the superimposed hydrostatic compressive stress component Y in Equation 4: (a) Y = 0, (b) Y = 0.2 and (c) Y = 0.5.

the z-axis approximately $0.5a$ beneath the surface. The lower plots, Fig. 2b and c, show the modified Tresca stress criteria contours when X = 0 and Y = 0.2 and 0.5 in Equation 4. Two differences are immediately obvious as Y increases to 0.5, namely that the value of the maximum shear stress decreases with increasing Y and the location of the maxima moves from $0.5a$ to approximately $0.8a$ beneath the surface of contact. Furthermore, the contours of shear stress are more arc-like from the diameter of contact; notice there is also a region directly beneath the contact area that is so influenced that yield is unlikely to occur because of the dominance of the hydrostatic compressive stresses in this region. Depending on the value of Y in Equation 4 the location and magnitude of the maximum shear stresses vary in a manner that is more complex than for simple uniaxial tensile or compressive tests. With increasing values of Y there is not a linear relationship with σ because of the differing gradients of P and σ with depth beneath the indenter. While the above demonstrates the situation for spherical tipped indenters, similar behaviour would be expected for conical, pyramidal and wedge shaped indenters.

Attempts to use the more rigorous relationships of Argon to model confined large strain (up to 100%) plastic deformation in compression tests and indentation of polycarbonate and PMMA polymeric materials using FEM methods has been recently pursued by Arruda and Boyce [18] and Jayachandran *et al.* [19].

In this paper our approach is more modest, in that we compare the uniaxial compressive response of a number of polymers with the behaviour beneath a spherical indenter. Initially the basis of the spherical indenter analysis is presented followed by details of the observations with both uniaxial compression and indentation approaches. The results are finally considered in the light of the spherical cavity model and the simple pressure dependence model of the yield stress mentioned above.

2. Experimental procedure

2.1. Background to spherical indentation

The basis for the interpretation of spherical indentation is derived from Hertz's [20] relationship between force and displacement or distance of mutual approach, namely

$$\delta = (3F/4E^*)^{2/3}/R^{1/3} \tag{6}$$

where δ is the displacement for a force, F; R is the indenter radius; and E^* the composite contact modulus of the indenter and substrate, which is given by

$$1/E^* = (1 - \nu_i^2)/E_i + (1 - \nu_s^2)/E_s \tag{7}$$

where the subscripts i and s refer to the indenter and substrate, respectively; and ν is Poisson's ratio. Provided the response of the material is elastic (that is, entirely reversible), the above relationship enables the determination of the modulus and contact pressure versus applied force. The averaged contact pressure is

given by

$$p_0 = F/\pi a^2 = F/\pi\delta(R - \delta/4) \quad (8)$$

where a is the radius of contact that may be determined with the knowledge that the contact circle depth, δ_c, lies at half the total depth of penetration (that is, $\delta/2$) and the use of Pythagoras' theorem.

Yield beneath a spherical indenter occurs at a contact pressure of $\sim 1.1\sigma_y$, where σ_y (for a metal) is the uniaxial tensile or compressive yield point at a localized region beneath the contact area. With increasing load the contact pressure increases and the plastic zone spreads and eventually intersects the surface. As the recent FEM analysis by Fischer-Cripps [14] indicates, the shape of the well developed plastic zone is highly dependent upon the σ_y/E ratio. A simple analysis of elastic–plastic force displacement curves generated with a spherical tipped indenter has been developed by Field and Swain [21]. A schematic illustration of the basis of this behaviour is shown in Fig. 3. A basic assumption underlying this approach is that the material behaves elastically during unloading. For polymeric materials this assumption may be severely compromised in tests close to the glass transition temperature.

The elastic response upon unloading along with the above mentioned relationship between contact depth, δ_c, and total penetration, δ_t, in Fig. 3c, enables the contact depth for elastic–plastic penetration to be written as

$$\delta_c = \delta_r + (\delta_t - \delta_r)/2 \quad (9)$$

where δ_r is the residual depth of the impression upon unloading. The contact pressure at maximum load is then given by

$$p_0 = F/\pi a^2 = F/\pi\delta_c(R - \delta_c) \quad (10)$$

The radius of the residual impression is given by

$$R_r = (a^2 + \delta_r^2)/2\delta_r \quad (11)$$

and the effective radius, R^*, of the indenter elastically unloading or reloading such a residual impression is given by

$$1/R^* = 1/R + 1/R_r \quad (12)$$

The elastic modulus may be determined from the elastic unloading portion of the force–displacement curve and for this elastic displacement, when $\delta \ll R$, the effective contact modulus is given by

$$E^* = 0.75\, F_{max}/a\delta_e \quad (13)$$

where $\delta_e = \delta_t - \delta_r$.

The elastic unloading response, resulting in δ_e being proportional to $F^{2/3}$, enabled Field and Swain [21] to develop an indenting procedure that included a partial unload step at various loads throughout a test, as shown schematically in Fig. 4. The knowledge of a force and displacement at some load prior to partial unloading and the determination of the partially unloaded force and displacement value enables the residual impression depth, δ_r, to be determined using the

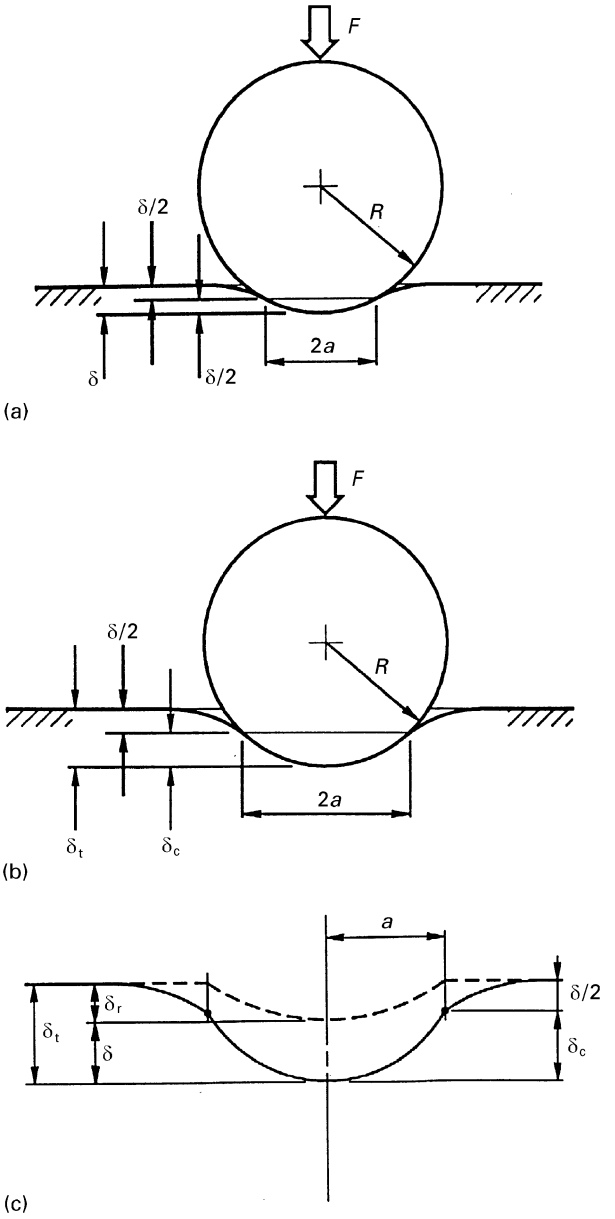

Figure 3 Schematic diagram of the deformation and definition of the various contact dimensions for a spherical indenter generating: (a) elastic contact, (b) elastic–plastic contact, and (c) the residual impression. F is the applied force, δ_t is the total penetration, δ_r the residual penetration and δ_c the peneration of the contact circle.

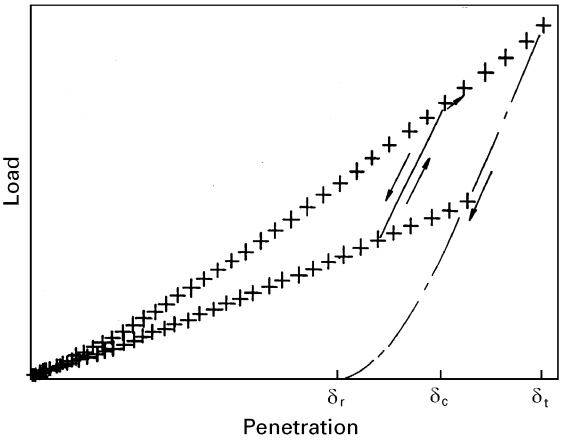

Figure 4 Schematic diagram illustrating the loading–partial–unloading indentation procedure with a spherical indenter, where h_t is the total penetration, h_p the partial penetration and h_r the residual penetration.

TABLE I Sample dimensions for compression testing

Sample	T_g (°C)	Formula	Sample dimensions (mm) ϕ = diameter (mm)		
			1	2	3
PMMA					
1	~ 114	$CH_2CCH_3COOCH_3$	3.41 × 8.19⌀	3.36 × 8.00⌀	3.36 × 8.34⌀
2			5.95 × 5.52⌀	5.95 × 5.46⌀	
3			4.69 × 12.58⌀	4.68 × 12.56⌀	4.69 × 12.56⌀
HDPE†	− 127	CH_2CH_2	3.28 × 7.82⌀	3.26 × 7.82⌀	3.24 × 7.84⌀
PET	~ 69	$COC_6H_4COOCH_2CH_2O$	3.34 × 5.60⌀	3.36 × 5.68⌀	
SAN††		$CH_2CHC_6H_4CH_2CHCN$	3.38 × 7.32⌀	3.4 × 7.78⌀	3.20 × 8.42⌀
PC†††	~ 149	$C_6H_4CCH_3CH_3C_6H_4OCO$	3.48 × 8.33⌀	3.46 × 8.31⌀	3.46 × 6.90⌀

†High density poly-ethylene
††Styrene acrylonitrile
†††Poly-carbonate

following

$$(F_m/F_i)^{2/3} = (\delta_m - \delta_r)/(\delta_i - \delta_r) \quad (14)$$

where F_m, δ_m are the maximum load and displacement prior to unloading to F_i, δ_i, respectively. In this manner the contact pressure and modulus may be ascertained almost continuously throughout the test.

The above approach relies on a constant value of the indenter radius, which is almost impossible to ensure for small radii polished onto the tips of diamond cones due to the crystallographic anisotropy of diamond. To overcome this problem Bushby *et al.* [22] investigated a variety of approaches to quantify the indenter tip shape. The simplest and most attractive was found to be the use of the partial unload procedure outlined above on a material of known elastic modulus and Poisson's ratio and indented entirely within the elastic regime. Then with the aid of Equation 4, the effective radius versus depth may be determined. Two attractive materials for such calibration measurements were found to be silica glass and glassy carbon.

2.2. Materials

The thermoplastic polymeric materials investigated were all machined from commercially prepared and available sheet samples, typically 2–5 mm in thickness. The materials along with their literature values of the glass transition temperature, T_g, are listed in Table I. For the compression tests, discs of 5.5–12.7 mm diameter were machined from these sheets. The microindentation tests were conducted on the same discs prior to compression testing. No attempt was made to polish or anneal the "as-received" samples prior to testing.

2.3. Uniaxial compression tests

Compression tests were performed with well aligned steel anvils loading onto the polymer samples. A clip gauge was connected across the samples directly attaching to the steel anvils to avoid machine compliance influences. Tests were performed at a constant cross-head speed of 0.5 mm min^{-1} until a strain of 15% was achieved then unloaded at the same rate as the loading. This loading rate was chosen because it approximated the test duration for the indentation tests. Three tests were performed for each material.

2.4. Indentation tests

All indentation tests were performed with the UMIS 2000 using the load–partial unloading procedure outlined in Section 2.1. A partial unload step of 50% of the maximum load for 30 increments of loading was used throughout the study. Tests were performed with the nominally 20 and 50 μm radius indenters. The indenters were calibrated by loading a glassy carbon material to comparable depths of penetration in the manner outlined above. The elastic modulus and Poisson's ratio of the glassy carbon were independently measured using ultrasonic methods and found to be 25 GPa and 0.135, respectively.

The calculated radius versus depth of contact is shown in Fig. 5, for the nominally 50 μm radius indenter. For both indenters the initial radii were well above the nominal value but they asymptotically approach the nominal value after a micrometre or more of penetration. These results were in good agreement with scanning electron microscope (SEM) observations of the indenter tips that in both instances appeared slightly flattened in the vicinity of the tip.

3. Results

3.1. Uniaxial compression tests

Representative examples of some of the compression tests are shown in Fig. 6. In many instances there was an initial gradual increase of the slope of the stress–strain curve, presumably due to asperities on

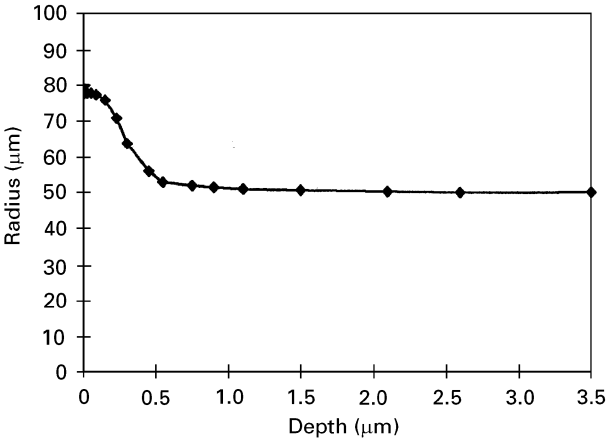

Figure 5 Calibrated radius versus contact depth for the nominally 50 μm radius diamond indenter.

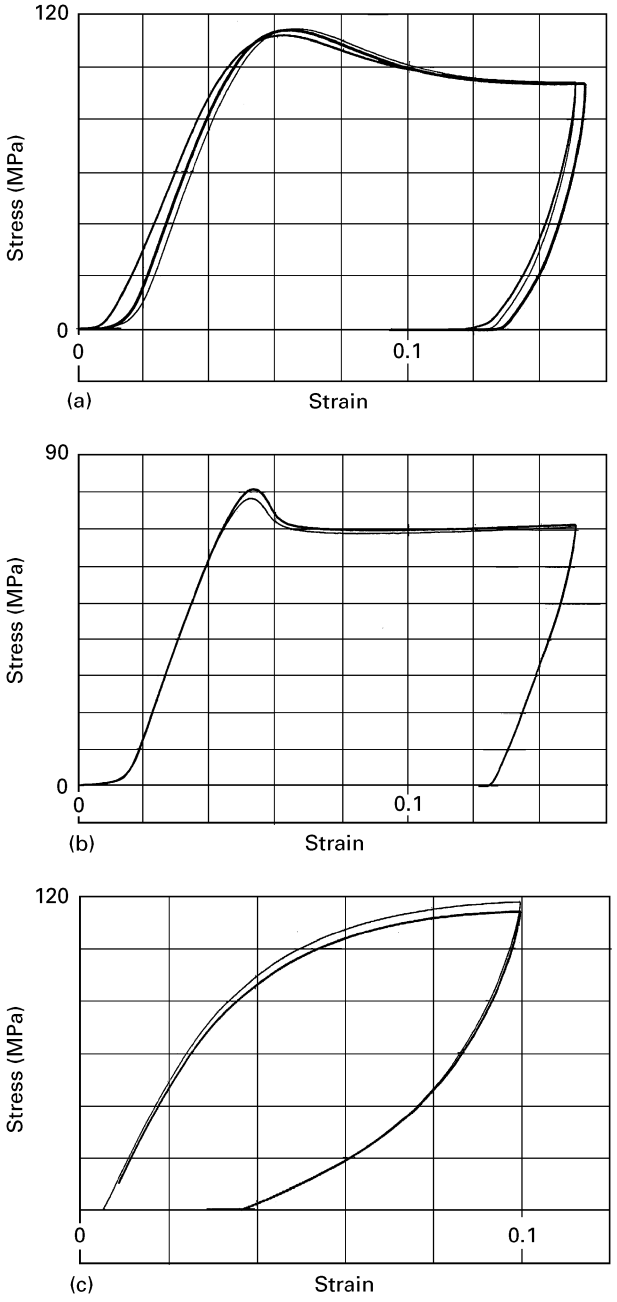

Figure 6 Stress–strain curves determined in uniaxial compression for the following polymeric materials tested: (a) SAN, (b) PET, and (c) PMMA 2.

the samples. In determinations of the stress–strain curve no allowance was made for the change in cross-sectional area during the test as the error associated with this omission was considered to be minimal for the limited plastic strain range investigated ($< 10\%$).

The modulus of the materials was estimated from the slope of the mid-section (20–70% of peak value) of the stress–strain curves for all the samples. The stress at 0.1 and 5% plastic strain of the stress–strain curve was also estimated. The measured values for the modulus and these yield stress values are shown in Table II along with the standard deviations of the modulus values.

3.2. Indentation tests

The UMIS indentation results displayed excellent consistency as shown in Fig. 7, which is the superposition of five sets of data for SAN (a), five for PET (b) and three for PMMA (c). Notice that in all the figures the data for the loading and unloading overlap at low loads and at higher values they begin to split because of the onset of plastic deformation of the polymers.

Determination of contact pressure and modulus versus depth as well as the indentation stress–strain curves followed the procedure outlined in Section 2.1. The analysis incorporated the change in effective radius as a function of penetration as shown in Fig. 5 for the nominally 50 μm radius indenter.

The calculated indentation stress–strain curves (contact pressure versus contact strain, a/R) for all these materials is shown in Fig. 8. The results show that there is always an initial elastic response then departure from that behaviour. The results shown in Table II list the measured elastic modulus from both approaches, compression and indentation tests, as well as the stress at the onset of yield (0.1% plastic strain) and at 5% plastic strain. In the case of the indentation tests the point of deviation from the elastic response as well as that at an indentation strain of 0.3 (a/R) is listed. Apart from the PET and SAN all the materials show significant hardening. Table II also includes the ratio of the indentation stress to compression yield stress values at comparable equivalent strains.

4. Discussion

The compression tests for the various polymers (Fig. 6) display a very similar response to typical published work [23] of, for example, PET and PMMA.

TABLE II Measured modulus and yield stress values obtained for compression (com) and (ind) indentation tests

Material	Compression			Indentation			Ratio	
	Modulus (GPa)	Yield stress, σ_y^{com} (MPa)		Modulus (GPa)	Yield stress σ_y^{ind} (MPa)		R, $\sigma_y^{ind}/\sigma_y^{com}$	
		0.1%	5%		0.1%	5%	0.1%	5%
HDPE	1.31 (0.16)	16	31	1.43 (0.06)	38	54	2.38	1.74
PC	1.66 (0.06)	51	75	2.43 (0.19)	105	155	2.08	2.08
PET	2.50 (0)	72	69.5	2.95 (0.19)	105	192	1.46	2.76
PMMA								
1	1.55 (1.08)	71	102	3.27 (0.09)	141	270	1.97	2.65
2	3.21 (3.17)	67	112	3.38 (0.07)	105	230	1.57	2.05
3	3.23 (0.06)	75	131	2.52 (0.06)	155	260	2.07	1.98
SAN	3.37 (0.29)	98	101	3.74 (0.22)	140	262	1.43	2.57
Average							1.85	2.26

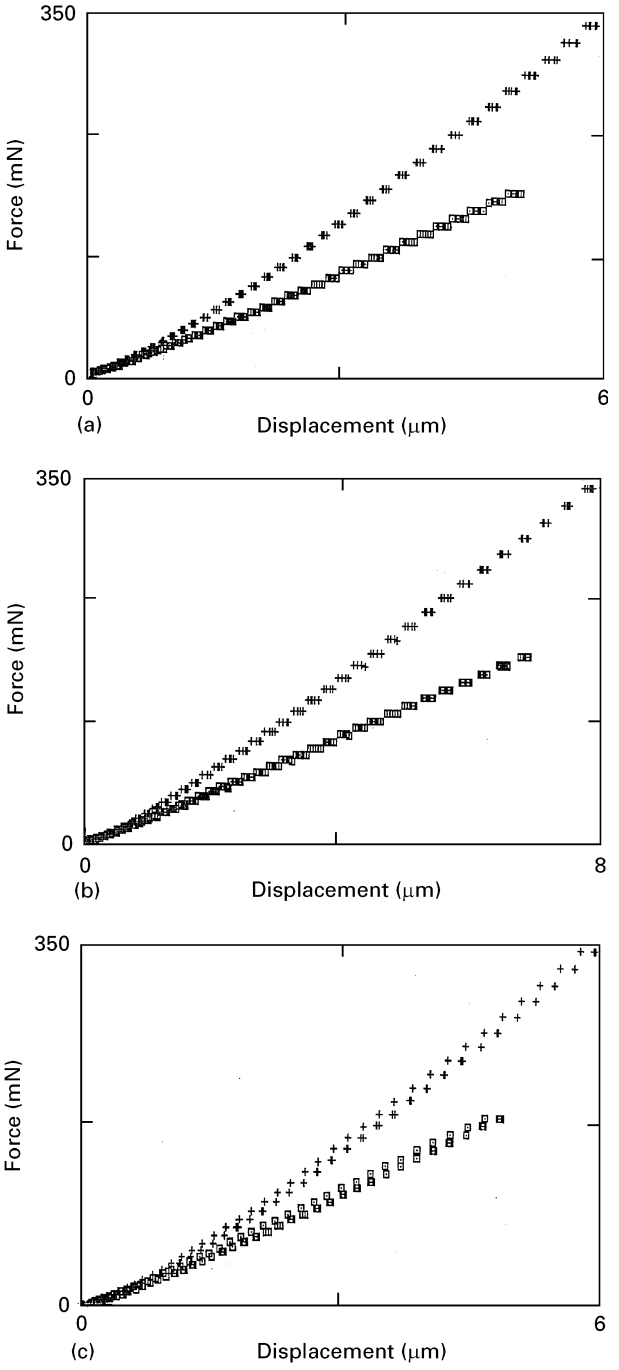

Figure 7 Typical load–partial unload test data for the nominally 50 μm radius indenter loaded into: (a) SAN, (b) PET, and (c) PMMA 2.

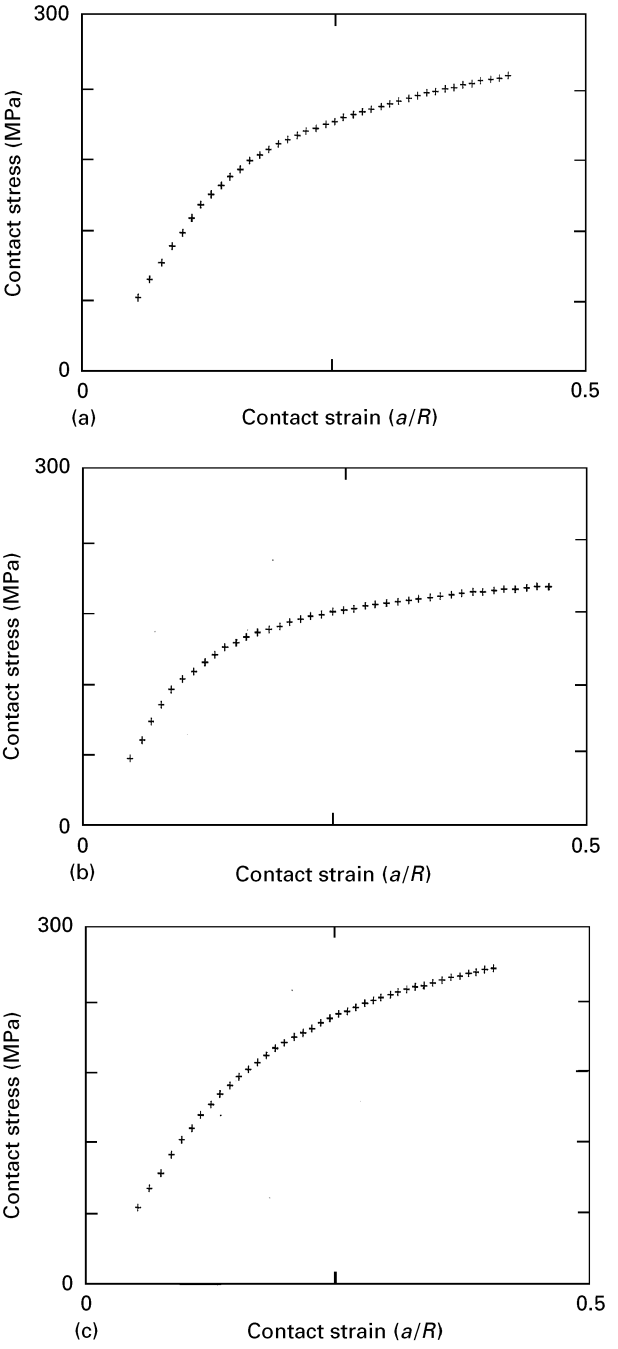

Figure 8 Indentation stress–strain curves (contact pressure versus a/R) for the following polymeric materials tested: (a) SAN, (b) PET, and (c) PMMA 2.

The modulus values, all estimated on the basis of literature Poisson's ratios, are in good agreement with accepted values. Of particular interest among these materials was that of PET, which showed a typical upper yield point (Fig. 6b) before exhibiting a plateau stress–strain behaviour. Associated with this load drop, the material changed from transparent to white opaque. The stress–strain response beyond the onset of yield for both the compression and indentation tests, particularly for the PMMA, and PC might have been better fitted to a Ramberg–Osgood relationship to account for the observed hardening.

The indentation observations, particularly the indentation stress–strain response, showed a similar form to those of the compression tests. The values of the moduli were in good agreement with those of the compression test whereas the yield stresses were always almost double those of the compression tests for comparable values of strain. The ratio of H to E (contact pressure to modulus) for the polymers from the results in Fig. 7 is not a fixed value but changes with increasing strain for most of the polymers.

The observations shown in Table II indicate that for nearly all the materials the ratio of indentation contact pressure to compression yield stress lies in the range from 1.8 to 2.3 over a wide range of plastic strains. In the present results, for most of the materials, the hardening response is evident in both the compression and indentation tests, the major exceptions being the PET and SAN. In previous studies of indentation contact pressure to higher values of a/R (up to 0.8) by Kent [17] for PMMA it was argued that the (rising)

value of the contact pressure was strongly dependent on the interfacial friction and if this was accounted for analytically then the form of the contact pressure versus a/R was almost constant. The values of contact pressure obtained by Kent are slightly higher than those measured here as he used a significantly higher stressing rate of loading.

An alternative approach for comparing the compression and indentation stress–strain results for the polymers is provided by the analysis of Argon [16]. As the testing was done at temperatures well below the glass transition temperature, with the exception of the HDPE and, furthermore, as both compression and indentation tests were conducted at comparable strain rates, then Equation 4 may be written as

$$\sigma_y = \sigma_{y0} + YP \tag{15}$$

with P the hydrostatic pressure (defined in Equation 5) and Y the dilability or compressibility coefficient. Typical values for Y are in the range from 0.15 to 0.4 for polymeric materials [18, 19]. The consequence of this approach is that, depending on the testing procedure, the value of the yield stress and subsequent stress–strain curve will change.

The plots of hydrostatic pressure influenced von Mises (Tresca) yield contour stresses shown in Fig. 2 and the values of the maximum shear stress determined, enable an estimate of the ratio of the yield stress under indentation to that in compression. For example, for values of $Y = 0.2$ and $Y = 0.5$ in Equation 15, the ratio of the yield stresses from Equation 15 is given by 1.11 and 1.53, respectively. In the case of the ratio of indentation yield stress to the tensile yield stress this ratio increases to 1.26 and 2.21, respectively. While it is known that the elastic modulus of polymers is also dependent on the hydrostatic stress, the significance of the localized nature of the very high contact pressures beneath a spherical indenter means that they influence the yield stress more than the elastic behaviour that is determined more by the far field integrated displacement throughout the substrate.

The present observations and those of Kent [17] indicate that care must be exercised when attempting to relate the indentation contact pressure or hardness to the yield stress of polymers as is typically done for metallic materials. Parameters that appear to be important are the localized confining pressure and the compressibility index of the materials and, although not investigated here, perhaps the interfacial friction between indenter and specimen.

5. Conclusions

The present observations have shown that spherical indentation using the load–partial–unload procedure is a simple and efficient method for determining the elastic and elastic–plastic response of a number of polymers well below their glass transition temperatures. The values obtained for the elastic modulus are in good agreement with generally accepted literature values and are comparable to the values measured using a traditional compression test, whereas the values obtained for yield stress are generally higher than compression measurements by a factor of 1.8–2.2. This type of difference is anticipated because of the compressive confining pressure influence on the yield behaviour of polymers as proposed by Argon [16]. However, the extent of the differences is a little higher than anticipated and this may be a consequence of interfacial friction between the indenter and specimen as suggested by Kent [17].

References

1. J. B. PETHICA, R. HUTCHINS and W. C. OLIVER, *Phil. Mag.* **48**, (1983) 593.
2. T. J. BELL, A. BENDELI, J. S. FIELD, M. V. SWAIN and E. G. THWAITE, *Metrologia* **28** (1990/91) 463.
3. R. P. BROWN, "Handbook of plastics test methods" (Longman, Harlow, 1988) Ch. 8.
4. B. J. BRISCOE and K. SAVIO SEBASTIAN, *Rubber Chem. Technol.* **66** (1993) 625.
5. R. H. ION, H. M. POLLOCK and C. ROGUES-CARMES, *J. Mater. Sci.* **25** (1990) 1444.
6. B. Y. NI, R. G. BISSON and A. H. TSOU, "Thin films: mechanical properties IV" edited by P. H. Townsend, T. P. Weihs, J. E. Sanchez and P. Borgensen, MRS Vol. **308** (1993).
7. D. TABOR, "Hardness of metals" (Clarendon Press, Oxford, 1951).
8. D. M. MARSH, *Proc. Roy. Soc. Lond.* **A279** (1964) 420.
9. R. J. HILL, "The mathematical theory of plasticity" Engineering Science Series (Clarendon Press, Oxford, 1950).
10. W. HIRST and M. G. J. W. HOWSE, *Proc. Roy. Soc. Lond.* **A311** (1969) 429.
11. K. L. JOHNSON, *J. Mech. Phys. Sol.* **5** (1970) 125.
12. M. C. SHAW and D. J. DESALVO, *J. Eng. Ind. Trans. ASME* **92** (1970) 469.
13. E. H. YOFFE, *Phil. Mag.* **A46** (1982) 617.
14. A. C. FISCHER-CRIPPS, *J. Mater. Sci.* **32** (1996) 727.
15. K. E. PUTTICK, L. S. A. SMITH and L. E. MILLER, *J. Phys. D: Appl. Phys.* **10** (1977) 617.
16. A. S. ARGON, *Phil. Mag.* **28** (1973) 839.
17. R. J. KENT, *J. Phys. D: Appl. Phys.* **14** (1981) 601.
18. E. M. ARRUDA and M. C. BOYCE, *Int. J. Plasticity* **9** (1993) 697.
19. R. JAYACHANDRAN, M. C. BOYCE and A. S. ARGON, *J. Adhesion Sci. & Technol.* **7** (1993) 813.
20. K. L. JOHNSON, "Contact mechanics" (Cambridge University Press, 1985).
21. J. S. FIELD and M. V. SWAIN, *J. Mater. Res.* **8** (1993) 297.
22. A. J. BUSHBY, T. J. BELL and M. V. SWAIN, in preparation.
23. P. B. BOWDEN and S. RAHA, *Phil. Mag.* **22** (1970) 463.

Received 27 November 1996
and accepted 10 February 1997